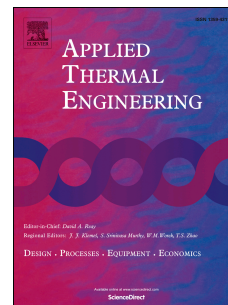


Accepted Manuscript

Performance analysis of a triple-effect absorption cooling cycle using aqueous (lithium, potassium, sodium) nitrate solution as a working pair

MaríaE. Álvarez, Xavier Esteve, Mahmoud Bourouis



PII: S1359-4311(15)00015-0

DOI: [10.1016/j.applthermaleng.2015.01.011](https://doi.org/10.1016/j.applthermaleng.2015.01.011)

Reference: ATE 6279

To appear in: *Applied Thermal Engineering*

Received Date: 21 July 2014

Revised Date: 3 December 2014

Accepted Date: 4 January 2015

Please cite this article as: M. Álvarez, X. Esteve, M. Bourouis, Performance analysis of a triple-effect absorption cooling cycle using aqueous (lithium, potassium, sodium) nitrate solution as a working pair, *Applied Thermal Engineering* (2015), doi: 10.1016/j.applthermaleng.2015.01.011.

This is a PDF file of an unedited manuscript that has been accepted for publication. As a service to our customers we are providing this early version of the manuscript. The manuscript will undergo copyediting, typesetting, and review of the resulting proof before it is published in its final form. Please note that during the production process errors may be discovered which could affect the content, and all legal disclaimers that apply to the journal pertain.

1 **Performance analysis of a triple-effect absorption cooling**
2 **cycle using aqueous (lithium, potassium, sodium) nitrate**
3 **solution as a working pair**

4 María E. Álvarez, Xavier Esteve, Mahmoud Bourouis*

5 Department of Mechanical Engineering, Universitat Rovira i Virgili, Av. Països Catalans No. 26,
6 43007 Tarragona, Spain

7 * Corresponding Author (Email: mahmoud.bourouis@urv.cat; Phone: +34 977 55 86 13; Fax: +34 977 55 96 91)

8
9 **Abstract**

10 A triple-effect absorption cooling cycle using aqueous (lithium, potassium, sodium) nitrate solution
11 (Alkitate) as a working fluid in the high temperature stage is simulated in this work. This cycle takes
12 advantage of the thermal potential of high temperature heat sources and has a configuration
13 consisting of a H₂O/LiBr double-effect cycle coupled with a single-effect cycle that uses Alkitate as a
14 working fluid. Heat is exchanged between the two cycles by thermal fluids which flow in the external
15 circuits. The conventional working fluid H₂O/LiBr suffers from serious problems of corrosion and
16 thermal decomposition at temperatures of over 180°C, which restricts its use in the high temperature
17 components of a triple-effect absorption cooling cycle. At the nominal operating conditions selected,
18 namely a heat source temperature T_H of 250°C and a cooling-water temperature T_C of 30°C the
19 coefficient of performance achieved with the Alkitate topping cycle is 1.73. The correct operation of
20 the cycle is demonstrated by drawing the cycle in the Duhring diagram, where the safety margin for
21 the crystallization of the working fluid is adhered to.

22 Results show that the Alkitate triple-effect cycle has a slightly higher efficiency as compared to the
23 H₂O/LiBr triple-effect cycle at generator temperatures of over 180°C. Moreover, the practical
24 operation of a H₂O/LiBr triple-effect cycle at temperatures higher than 180°C suffers from the
25 abovementioned problems related to the thermal stability and corrosion of the working pair.

26 **Keywords:** triple-effect absorption cycle, aqueous nitrate solution, alkitate, high-temperature heat
27 sources.

28 **Highlights**

- 29 ○ A triple-effect absorption cooling cycle using Alkitate as a working pair is simulated for high
30 temperature heat sources.
- 31 ○ The cycle configuration consists of a H₂O/LiBr DE cycle coupled with a SE cycle using Alkitate
32 as a working fluid.
- 33 ○ The Alkitate TE cycle has a slightly higher COP compared to H₂O/LiBr TE cycle at generator
34 temperatures of over 180°C.
- 35 ○ The Alkitate triple-effect cycle represents a feasible and efficient configuration for high
36 temperature heat sources

38 **1. Introduction**

39 Triple-effect absorption cooling cycles take advantage of the thermal potential of high temperature
40 heat sources and can achieve a coefficient of performance (COP) of up to 50% more than the
41 conventional cooling systems with double-effect cycles [1]. Several authors proposed different
42 configurations of triple-effect absorption cooling cycles. These configurations were often
43 characterized in terms of the number of thermal components. A multi-stage absorption cooling

44 system comprising several generator/condenser stages and at least one single-stage
45 evaporator/absorber was patented by Mamiya [2]. Oouchi et al. [3] patented a triple-effect cooling
46 system with three generators parallel with each other, in which the solution was supplied from the
47 absorber directly to each of these three generators. Ziegler et al. [4] estimated the performance of
48 seven different configurations of triple-effect cycles for chilling and refrigeration applications. These
49 cycles were formed by the superposition of single-effect cycles and consisted of seven or eight
50 thermal components. Grossman et al. [5] simulated several configurations of H₂O/LiBr triple-effect
51 cycles in a wide range of operating conditions. The systems analysed included the three-condenser-
52 three-generator cycle, to form an extension of the conventional double-effect cycle, and two cycles in
53 which additional heat recovered from the condensate leaving the highest temperature condenser
54 was supplied to the lowest temperature generator. These two cycles were called Double Condenser
55 Coupled (DCC) cycles since heat recovered from the highest temperature condensed refrigerant was
56 used to heat both the middle temperature generator (heat of condensation) and the lowest
57 temperature generator (subcooling of the condensed refrigerant).

58 Garimella et al. [6] investigated a triple-effect absorption heat pump using NH₃/H₂O as a working fluid
59 in the higher pressure cycle, while NH₃-H₂O and NH₃/NaSCN solutions were studied for the low
60 pressure cycle. The cycle configuration was such that the heat duties of the absorber, condenser
61 and rectifier of the high pressure cycle were rejected to the generator of the low pressure cycle.

62 Kaita [7] performed a simulation analysis of three configurations of the H₂O/LiBr triple-effect
63 absorption cooling cycle, corresponding to different flow arrangements i.e. parallel-flow, series-flow
64 and reverse flow.

65 Wang et al. [8] proposed the integration of an exhaust heat recovery generator with conventional
66 gas-fired triple-effect H₂O/LiBr absorption cooling cycles to improve the energy efficiency of the
67 system. The results showed that the coefficient of performance of the system was increased from

68 1.78 to 1.83. The authors concluded that this technology could be easily implemented and could
69 provide desirable economic benefits, which would be feasible in the development of triple-effect
70 absorption cycles.

71 Gebreslassie et al. [9] determined the coefficient of performance (COP), the exergetic efficiency, the
72 exergy destruction rate and evaluated the effect of the heat source temperature for seven different
73 configurations of simple, double, triple and half effect H₂O/LiBr absorption cycles. The COP obtained
74 significantly increased from half-effect to triple-effect cycles. The exergetic efficiency showed a less
75 pronounced variation between the different configurations. At higher heat source temperatures the
76 COP decreased slowly. The same qualitative behavior was observed for the exergetic efficiency but
77 the decrease at higher heat source temperatures was more significant. The exergy destruction rate
78 of the heat exchangers increased with the heat source temperature for the absorber and generator,
79 but was practically independent of the heat source temperature for the condenser and solution heat
80 exchanger.

81 Gomri [10] investigated the potential of H₂O/LiBr single, double and triple-effect absorption cycles for
82 chilled water production. The effects of different operation parameters on the coefficient of
83 performance, exergetic efficiency and the ratio of refrigerant generated to the heat supplied in the
84 generator were investigated by numerical simulation. The author concluded that the COP of the
85 triple-effect cycle was almost three fold that of the single-effect cycle. The results also showed that
86 when the evaporation temperature was varied between 4 °C and 10 °C and the condenser and
87 absorber temperatures were varied from 33 °C to 39 °C the maximum COP values of the triple-effect
88 absorption cycle were in the range 1.62-1.90.

89 Matsushima et al. [11] developed a dynamic simulation program to predict the transient behaviour of
90 absorption chillers with different cycle configurations. This simulation program was used in the
91 development phase of a high efficiency triple-effect absorption chiller. The results obtained showed

92 that this machine could be operated smoothly without significant problems and reached COP values
93 of over 1.6.

94 Agrawal and Karimi [12] proposed a triple-effect cycle which combined the advantages of absorption
95 cycle, ejector cycle and low temperature N_2O refrigerant based compression cycle. The authors
96 concluded that the cycle configuration proposed could produce refrigeration output at different
97 temperatures simultaneously.

98 Yabase and Makita [13] proposed a solar cooling system employing a steam-driven triple-effect
99 absorption chiller. The cooling system consisted of a triple-effect absorption chiller, a solar thermal
100 collector, a backup boiler, and accessory devices. The steam-driven triple-effect absorption chiller
101 was based on the direct-fired triple-effect absorption chiller developed by Japanese manufacturers
102 between 2001 and 2005 in which only the high temperature generator was modified from a boiler to
103 a heat exchanger for steam heat recovery. The proposed solar cooling system was compared with
104 existing solar thermal cooling systems including those using gas-fired and steam double-effect
105 absorption chillers and gas-fired triple-effect absorptions chillers and its superiority was
106 demonstrated.

107 Geng and Liu [14] performed an exergy analysis of a compressor assisted triple-effect absorption
108 refrigeration cycle. The authors reported that the addition of a compressor between the low pressure
109 generator and the condenser was an effective solution to reduce the heat source temperature
110 required and to mitigate the corrosion problem in counter-series triple-effect $H_2O/LiBr$ absorption
111 refrigeration cycles.

112 Agrawal et al. [15] proposed a solar driven triple-effect absorption refrigeration cycle for the
113 production of cooling at temperatures ranging from $-80^\circ C$ to $-50^\circ C$. The cycle configuration
114 integrated an ejector, absorption and cascaded refrigeration cycles. The effect of several design

115 parameters on energy and exergy performances of the proposed cycle was analysed. The authors
116 concluded that their results could be used to perform a suitable thermodynamic design of solar-
117 assisted triple-effect absorption refrigeration systems.

118 Therefore, different configurations can be obtained by changing the number of components or loops
119 to establish different couplings between the components and thus allow the use of a different
120 working fluid in each loop. Thereby, a corrosive absorbent can be restricted where it is required
121 within a certain loop, while other working fluids can be employed in other loops [1].

122 The conventional working fluid $\text{H}_2\text{O}/\text{LiBr}$ suffers from serious problems of corrosion and thermal
123 decomposition at the operating conditions of the triple-effect absorption cooling cycles. The mixture
124 $\text{H}_2\text{O}/\text{LiBr}$ is corrosive at temperatures of over 180°C and this makes it necessary to use high
125 temperature corrosion inhibitors and specific construction materials which are costly and may affect
126 the absorption process. The corrosion and thermal instability of the $\text{H}_2\text{O}/\text{LiBr}$ working fluid restricts its
127 use in the high temperature components of a triple-effect cycle.

128 On the other hand, Howe and Erickson [16] determined that the working fluid mixture called Alktrate
129 is compatible with austenitic stainless steel materials at high temperatures of up to approximately
130 260°C . This fluid mixture is composed of water as a refrigerant and the salt mixture
131 $\text{LiNO}_3+\text{KNO}_3+\text{NaNO}_3$, as absorbent with mass compositions of 53%, 28% and 19%, respectively.

132 However, this working fluid mixture does not exhibit a wide range of solubility, and consequently its
133 use at low temperatures is limited due to crystallization problems [1]. Therefore, Erickson et al. [1]
134 suggested that Alktrate could be used in the high temperature components of triple-effect absorption
135 cooling cycles, while the conventional working fluid $\text{H}_2\text{O}/\text{LiBr}$ could be used in the low temperature
136 components.

137 The objective of this work is to investigate the possibility of improving the use of the thermal potential
138 of high temperature heat sources, by simulating a triple-effect absorption cooling cycle using
139 aqueous (lithium, potassium, sodium) nitrate solution as a working fluid in the high temperature
140 stage. The operating principles of the selected absorption cooling cycles and the thermodynamic
141 simulation methodology are described. The effect of the heat source temperature (T_H) and cooling-
142 water temperature (T_C) on the performance of the Alktrate triple-effect cycle is also analysed.
143 Moreover, a comparative analysis of the theoretical performance of the Alktrate triple-effect cycle is
144 made with the $H_2O/LiBr$ triple-effect cycle at different operating conditions.

145 **2. Triple-effect absorption cooling cycle using aqueous nitrate solution as a working fluid**

146 2.1. Cycle configuration

147 Erickson et al. [1] investigated different triple-effect cycle configurations. In their study, the most
148 promising triple-effect cycle configurations were identified using qualitative selection criteria such as
149 operating pressure, solubility requirements of the working fluids, generic values of the coefficient of
150 performance (COP) estimated according to the superposition principle described by Alefeld and
151 Radermacher [17], risks involved in the component design and the number of components exposed
152 to a high corrosive environment. Based on their analysis, the authors [1] proposed a triple-effect
153 cycle with a high temperature stage using the aqueous (lithium, potassium, sodium) nitrate solution
154 (Alktrate) as a working fluid. They considered this cycle, known as the "Alktrate topping cycle", one
155 of the best performing configurations. This triple-effect absorption cooling cycle consists of a
156 $H_2O/LiBr$ double-effect cycle in parallel flow configuration, and a single-effect cycle using Alktrate as
157 a working fluid. The aqueous nitrate solution is limited to use in the high temperature stage because
158 it does not offer a wide solubility range. Its use at low temperatures is therefore non-viable due to
159 crystallization problems. The triple-effect cycles require high operating temperatures at which the
160 conventional working fluid $H_2O/LiBr$ cannot operate without the addition of corrosion inhibitors or the

161 use of costly resistant materials, besides presenting problems of thermal instability. Therefore,
162 Alktrate could be used in the high temperature components, while the conventional working fluid
163 H₂O/LiBr could be used in the lower temperature components of a triple-effect cycle.

164 In this study, a triple-effect absorption cooling cycle based on the configuration proposed by Erickson
165 et al. [1] has been selected. In this cycle configuration none of the components are exposed to
166 corrosion. The coupling details between the two cycles are discussed below.

167 2.2. Operating principles

168 In the conventional triple-effect cycles the heat rejected in the refrigerant condensation process is
169 used to activate the low pressure generator. Based on this and in order to achieve the integration of
170 the high temperature single-effect cycle and the double-effect cycle, two coupling loops are defined
171 as shown in Figure 1 and described below:

- 172 ○ Coupling loop 1: the heat rejected in the high temperature condenser and absorber (Alktrate
173 single-effect cycle) is used to drive the middle temperature generator (high pressure level in the
174 H₂O/LiBr double-effect cycle).
- 175 ○ Coupling loop 2: the heat rejected in the middle temperature condenser (high pressure level in
176 the H₂O/LiBr double-effect cycle) is used to drive the low temperature generator and to
177 evaporate the refrigerant in the evaporator of the Alktrate single-effect cycle.

178 These two coupling loops are made to work by heat exchange of the thermal fluids flowing in the
179 external circuits.

180 The Alktrate topping cycle consists of 23 components and 56 streams. The absorber ABS(2) and the
181 condenser CND(6) are cooled by means of external circuits, while the generator GEN(13) is
182 externally heated by the high temperature heat source. Chilled water is produced in the evaporator

183 EVP(1). Heat rejected in the condenser CND(5) is divided into two streams. To drive the generator
184 GEN(3) on the one side and on the other side to evaporate the refrigerant in the evaporator EVP(11).
185 The coupling between these three components CND(5), GEN(3) and EVP(11) is achieved with a
186 heat exchange circuit (coupling loop 2), in which the cooling water leaving the condenser is split into
187 two streams that later flow through the external circuits of the generator and the evaporator. In the
188 coupling loop 1 the heat rejected in the condenser CND(14) and the absorber ABS(12) of the
189 Alktrate single-effect cycle is used to drive the generator GEN(4) in the double-effect cycle. The
190 cooling-water streams leaving the external circuits of the condenser and the absorber of the high
191 temperature single-effect cycle are mixed and then sent to the external circuit of the high
192 temperature generator of the double-effect cycle.

193 The configuration of the double-effect cycle forming part of the selected triple-effect cycle
194 corresponds to the cycle configuration proposed by Grossman et al. [6] and consists of parallel flow
195 alternatively coupled condensers (Figure 1). The hot condensate leaving the condenser CND(5) and
196 the superheated steam from the generator GEN(3) are mixed together before entering the condenser
197 CND(6). The solution rich in refrigerant leaving the absorber ABS(2) is divided into two streams
198 before entering the generators GEN(3) and GEN(4) [6].

199 **3. Simulation methodology**

200 The operation and performance of the triple-effect absorption cooling cycle with a high temperature
201 single-effect stage using Alktrate as a working pair were analysed using the ABSIM (Modular
202 Simulation of Advanced Absorption Systems) program. ABSIM was selected as a simulation tool
203 because it is a specific modular program for absorption systems and was successfully used by
204 several researchers to simulate a variety of absorption systems with different multi-staged
205 configurations and different working fluids [18]. New subroutines containing the thermophysical
206 properties of the working fluids used in this work were developed and integrated into the ABSIM

207 properties database. The properties of the working fluid $\text{H}_2\text{O}/(\text{LiNO}_3+\text{KNO}_3+\text{NaNO}_3)$ with mass
208 compositions in salts of 53%, 28% and 19%, respectively, were then incorporated into the ABSIM
209 program. This program offers the possibility of updating the thermophysical properties of the working
210 fluids already available in the database. The flexibility of ABSIM allowed for the modification of the
211 aqueous nitrate solution properties in accordance with the research carried out by Alvarez in his
212 doctoral thesis [19].

213 Figure 2 shows a schematic diagram of the Alktrate triple-effect absorption cooling cycle created in
214 the ABSIM environment. The external coupling loops can be appreciated in this diagram. The
215 streams numbered 15, 16, 45, 46, 51 and 52, the mixer MIX(21) and the splitter SPL(20) form the
216 coupling loop 1, while the coupling loop 2 consists of the streams numbered 10, 11, 48, 49, 54 and
217 55, the mixer MIX(23) and the splitter SPL(22).

218 3.1. Problem definition in the ABSIM environment

219 Since the operation of each absorption cooling cycle depends on a number of operating conditions
220 and design parameters, the approach considered in the cycle simulations carried out in this work
221 was to establish a reference operation point for the system and vary the relevant parameters around
222 it. Furthermore, the design features, particularly the size of the heat exchange surfaces in the cycle
223 components (evaporators, generators, condensers, heat exchangers and absorbers), are a
224 determining factor in the cycle performance.

225 In previous studies Gommed and Grossman [20] selected a reference case consisting of a $\text{H}_2\text{O}/\text{LiBr}$
226 single-effect absorption chiller and tested it extensively. An extension of this study was carried out by
227 Grossman et al. [5] using the same approach for triple-effect absorption cooling cycles. Based on the
228 above, a reference case was defined in this work for the triple-effect cycle with a high temperature
229 stage operating with Alktrate as a working fluid (Figure 2). The values for the size, expressed in

230 terms of UA values of the evaporator, absorber, condenser, generators, and heat exchangers, are
231 those reported by Grossman et al. [5] and also for the external circuit flows, as well as for the
232 components operating with the aqueous nitrate solution as a working fluid. Actually, this
233 consideration is not completely correct, even if the heat transfer areas (A) remain constant, the
234 overall heat transfer coefficients (U) characterizing the heat transfer process taking place in the
235 thermal components vary depending on the working fluid and the operating temperatures. However,
236 selecting the reference case makes it possible to obtain a good approximation of the real case, since
237 the variation of the overall heat transfer coefficients (U) is relatively small in most cases and it also
238 allows for comparison of the results obtained for the triple-effect cycle under study with other
239 absorption cooling cycles. For a better understanding of the combined heat and mass transfer
240 governing the absorption and desorption processes, the variation of the UA values with relation to
241 the working fluid and operating temperatures should be considered [5].

242 Input data for simulating the triple-effect cycle with a high temperature stage using Alktrate as a
243 working fluid are listed in Table 1. They include the flow rates and temperatures in the external
244 circuits, the chilled water flow rate, the flow rate of the solution rich in refrigerant leaving each
245 absorber and the UA values.

246 The flow rate of the solution rich in refrigerant leaving the absorber ABS(2) is divided equally
247 between the streams sent to generators GEN(3) and GEN(4), as established in Table 1. Based on
248 this and in order to maintain the same solution flow rate at the generator entrance of each pressure
249 stage, the flow rate of the solution leaving the Alktrate absorber ABS(12) was set at $0.225 \text{ kg}\cdot\text{s}^{-1}$.

250 With this input data, the simulation code calculated the internal temperatures, flow rates,
251 concentrations, and other operating parameters at all the cycle streams at which the cycle
252 performance parameters were calculated.

253 The independent variables selected for simulating the triple-effect absorption cooling cycle with a
 254 high temperature Alktrate stage are as follows:

- 255 ○ The thermal activation energy is supplied to the upper stage generator GEN(13); hence the
 256 temperature of the stream 35 is known, $T_{35} = 250$ °C.
- 257 ○ The outlet temperature of the chilled water (stream 29) is set at 7.2 °C. The cooling effect (chilled
 258 water) takes place in the evaporator of the first stage EVP(1).
- 259 ○ The heat rejected in the thermal components is dissipated by means of cooling-water streams.
 260 Thus, the temperature of the cooling-water entering the condenser CND(6) and the absorber
 261 ABS(2) is known, $T_{23} = T_3 = 30$ °C.

262 3.2. Mathematical modelling

263 ABSIM was employed as a simulation tool in the present work. It incorporates a mathematical
 264 model based on mass and energy balances, heat and mass transfer equations, equilibrium
 265 considerations and the properties of the working fluids. Each component of the absorption cycle
 266 is treated as a control volume, with its own inputs and outputs that can be connected to other
 267 components. The governing equations applied to each component as well as the global equations
 268 are based on some or more of the following physical laws [5]:

269 a. Conservation of total mass:

$$270 \quad \sum_i m_i = 0 \quad (1)$$

271 where m_i is the mass flow rate ($\text{kg}\cdot\text{s}^{-1}$) of the stream numbered (i) in the absorption cycle.

272 b. Conservation of absorbent:

$$273 \quad \sum_i (m_i \cdot x_i) = 0 \quad (2)$$

274 where x_i refers to the total salt mass fraction of the stream (i)

275 c. Energy balance:

$$276 \quad \sum_i [(m_i \cdot h_i)_{in} - (m_i \cdot h_i)_{out}] + Q_{component} = 0 \quad (3)$$

277 h_i is the specific enthalpy of the solution ($\text{kJ} \cdot \text{kg}^{-1}$) of the stream (i) and $Q_{component}$ is the heat duty of
278 the component.

279 d. Heat transfer was expressed as follows:

$$280 \quad Q_{component} - UA * LMTD = 0 \quad (4)$$

281 where UA values were user-supplied inputs to describe the heat transfer characteristics. The heat
282 duty and logarithmic mean temperature difference, namely $Q_{component}$ and LMTD were calculated
283 according to the temperatures in each component of the absorption cycle.

284 e. Vapour-liquid equilibrium was defined by the pressure-temperature-concentration (P-T-X)
285 relationship:

$$286 \quad f(P_i, T_i, x_i) = 0 \quad (5)$$

287 P_i and T_i refer to the equilibrium pressure and temperature of the stream (i) at salt mass fraction x_i .

288 f. Mass transfer expressed in terms of a temperature deviation from equilibrium (DEV):

$$289 \quad T_i = T_{iE}(P_i, x_i) + DEV \quad (6)$$

290 where T_{iE} is the equilibrium temperature and DEV is the parameter that measures the deviation of
291 the vapour and liquid phases from the equilibrium conditions.

292 From the above equations of each component, a set of nonlinear equations was formed for the
293 whole system and then solved simultaneously.

294 To carry out the simulation, a number of assumptions that allow for the evaluation of the selected
295 absorption cooling cycles were considered. As mentioned before, the UA values of the thermal
296 components were obtained from a H₂O/LiBr absorption cooling cycle. Additional assumptions,
297 commonly made in this type of thermodynamic modeling, are:

- 298 ○ Steady state conditions are assumed,
- 299 ○ The kinetic and potential energies are negligible,
- 300 ○ Pressure drops along the pipelines and in components are neglected.
- 301 ○ Heat gains or losses to the surrounding along the pipelines and in components are
302 neglected.
- 303 ○ Solution streams leaving the generators and absorbers are in saturated conditions,
- 304 ○ Refrigerant streams leaving the evaporators and condensers are in saturated conditions,
- 305 ○ Enthalpy of the fluid entering the expansion valve is equal to its enthalpy in the valve exit.

306

307 3.3. Operating parameters of the triple-effect absorption cooling cycle

308 The cycle analysis was performed in terms of the coefficient of performance (COP), cooling capacity
309 (Q_E), circulation ratio (CR) and the risk of crystallization of the working fluid mixture.

310 The coefficient of performance of the cycle (COP) was defined as the ratio of the thermal load
311 (cooling capacity, Q_E) in the evaporator EVP(1) producing the desired cooling effect to the heat

312 supplied to the high temperature generator externally heated GEN(13) ($Q_{\text{GEN}(13)}$). The consumption
313 of the solution pumps and heat losses were not considered. The mathematical formulation of this
314 parameter for the absorption cooling cycle under study is:

$$315 \quad \text{COP} = \frac{Q_E}{Q_{\text{GEN}(13)}} \quad (7)$$

316 The circulation ratio (CR) or flow ratio between the solution rich in refrigerant and the refrigerant
317 entering the absorber is a parameter that provides information on the amount of solution which is
318 needed to absorb $1 \text{ kg}\cdot\text{s}^{-1}$ of refrigerant vapour in the absorber. A high value of CR indicates that
319 mass concentrations of the rich and poor solutions are very close, and therefore it is necessary to
320 circulate a high flow rate of the solution to absorb the refrigerant vapour mass flow rate of a given
321 cooling capacity. A high value of CR is not suitable because it implies that more pumping power is
322 required to circulate the solution and that the pipe diameters should be greater. It also indicates that
323 sensible heat losses taking place in the solution heat exchangers are greater.

324 The risk of crystallization of the working fluid in an absorption cooling cycle is evaluated by the
325 difference between the temperature (T_{44}) of the solution poor in refrigerant leaving the solution heat
326 exchanger HEX(15) and the crystallization temperature corresponding to the solution concentration
327 at this point ($T_{\text{cris}}(X_{44})$).

328 Indeed, the risk of crystallisation of the working fluid is higher at the heat exchanger exit of the circuit
329 using the solution poor in refrigerant because this is where the solution with the highest
330 concentration in salt is at its lowest temperature. A safety margin of $10 \text{ }^\circ\text{C}$ was selected to prevent
331 crystallisation at this point of the cycle.

332

333

334 4. Results and discussion

335 The simulation results of the Alktrate topping cycle together with a comparison with the triple-effect
336 cycle using H₂O/LiBr as a working fluid are presented in this paragraph.

337 4.1. Alktrate topping cycle

338 We evaluated the performance of a triple-effect absorption cooling cycle formed by the coupling of
339 two separate cycles, namely a double-effect cycle operating with the conventional working fluid
340 H₂O/LiBr and a single-effect cycle that operates at high temperatures with the working fluid
341 H₂O/(LiNO₃+KNO₃+NaNO₃) with mass ratios in salts of 53:28:19, respectively.

342 The simulation results of the Alktrate topping cycle represented in Figure 2 at the operating
343 conditions specified in Table 1 are shown in the Duhring diagram of Figure 3. This diagram is very
344 useful because it allows for visualization of the cycle circuits and the relative positions of the thermal
345 components and facilitates the understanding of the cycle operation and direct observation if the
346 operating conditions of the cycle violate the limits of the design. As observed in Figure 3, the Alktrate
347 topping cycle operates at 4 levels of pressure. Crystallization lines of the aqueous solutions of
348 H₂O/LiBr [21] and nitrates (Alktrate) [22] were included in the Duhring diagram in order to observe
349 the areas for solubility of both working fluids. Indeed, a drawback of the Alktrate working pair is its
350 limited solubility. However, in the stream number 44 at the exit of the solution heat exchanger
351 HEX(15) where the solution has the highest concentration in salt (91.01 wt%) and the lowest
352 temperature in the whole circuit of the solution poor in refrigerant, no risk of crystallization is
353 appreciated. The temperature of stream 44 is 11°C above the crystallization temperature of the
354 solution, as observed in Figure 3. These operating conditions ensure that the operation of the cycle
355 is feasible, although the safety margin for salt crystallization in the cycle is narrow.

356 The results obtained for the reference case showed that the triple-effect cycle with Alktrate has a
357 coefficient of performance (COP) of 1.73, a cooling capacity of 55.39 kW and a circulation ratio of
358 18.57 for the H₂O/LiBr double-effect cycle (CR_{LiBr}) and of 19.09 for the Alktrate single-effect cycle
359 (CR_{Alk}) without risk of crystallization ($T_{44}-T_{crist} = 11.2^{\circ}\text{C}$).

360 Figure 4 shows the coefficient of performance (COP) of the Alktrate topping cycle as a function of
361 the heat supply temperature T_H (stream 35) in the externally heated generator GEN(13) at three
362 different values of the cooling-water temperature T_C (streams 3 and 23), keeping the remaining
363 parameters constant. The cycle performance curves exhibit typical behavior for absorption cooling
364 cycles, the COP increases as the heat supply temperature T_H increases and decreases with the
365 increase in the cooling-water temperature T_C . When the activation temperature reaches the minimum
366 temperature required for the cycle operation, the COP increases sharply then stabilizes to a constant
367 value at a higher temperature and even decreases slightly with a further increase in the heat supply
368 temperature. The values of T_H for which an asymptotic trend of the COP curves was obtained are
369 170° , 190° and 250°C at cooling-water temperatures T_C of 25° , 30° and 35°C , respectively. Figure 4
370 represents the lines corresponding to the temperature of the solution poor in refrigerant at the exit of
371 the solution heat exchanger HEX(15) (stream 44) and the crystallization temperature corresponding
372 to the current concentration of this stream. These lines illustrate that an increase in the heat source
373 temperature T_H reduces the difference between the current operation temperature of stream 44 and
374 the corresponding crystallization temperature which, in turn, increases the risk of crystallization of the
375 solution. Moreover, Figure 4 shows that the maximum temperature at which the generator can
376 operate safely without the risk of the solution crystallizing is 260°C . The risk of crystallization is lower
377 for the rest of the operating conditions.

378

379

380 4.2. Comparison with cycles employing H₂O/LiBr as a working fluid

381 The results obtained with the Alkitate topping cycle were compared with the results obtained from
382 previous studies for triple-effect absorption cooling cycles using H₂O/LiBr as a working fluid.
383 Concretely, a comparison was made between the H₂O/LiBr triple-effect cycle proposed by Grossman
384 et al. [5] (Figure 5) and the Alkitate topping cycle in which the flow arrangement in the H₂O/LiBr
385 double-effect cycle is in series (Figure 6).

386 The input data in Table 1 was adapted to each cycle configuration. The coefficient of performance
387 (COP) and cooling capacity of each cycle were used as parameters for comparison. Figures 7 and 8
388 show the trends of the performance parameters in each cycle configuration depending on the heat
389 source temperature T_H . The temperatures of the chilled water and cooling-water entering ABS(2) and
390 CND(6) were set at 7.2° and 30°C, respectively. In all the cycle configurations investigated, the
391 mass flow rate of the solution leaving the absorber ABS(2) was set at 0.45 kg.s⁻¹ and an equal
392 distribution was used for the solution flow rate entering the middle temperature and high temperature
393 generators.

394 According to the COP curves, the Triple-effect cycle using H₂O/LiBr as a working fluid shows COP
395 values greater than those of the Alkitate topping cycle up to T_H of 180°C, and from then on COP
396 trends are slightly inverted as T_H increases leading to a higher performance of the Alkitate topping
397 cycle with a parallel flow configuration compared to the H₂O/LiBr triple-effect cycle. Likewise, the
398 results obtained in previous studies regarding the flow arrangement are confirmed. The parallel flow
399 arrangement represents an improvement of approximately 20% in the COP of the cycle as compared
400 to the series flow arrangement.

401 Cooling capacity usually follows an opposite trend in behaviour to that of COP, therefore COP
402 maximization actually results in a reduction of the cooling capacity. However, the reduction of the

403 cooling capacity in the Alkitate topping cycle is more significant as compared to the H₂O/LiBr triple-
404 effect cycle. On the other hand, the operation of H₂O/LiBr triple-effect absorption cooling cycles at
405 temperatures of over 180°C suffers from serious problems related to thermal stability and corrosion
406 of the working pair, so the feasibility of using H₂O/LiBr triple-effect cycles for high temperature heat
407 sources depends on the development of new construction materials or corrosion inhibitors that allow
408 for the above mentioned obstacles to be overcome.

409 Therefore, the triple-effect cycle with a high temperature Alkitate stage represents a feasible and
410 efficient option that allows for the thermal potential of high temperature heat sources to be taken
411 advantage of.

412 5. Conclusions

413 The triple-effect absorption cooling cycle called the "Alkitate topping cycle" which uses aqueous
414 (lithium, potassium, sodium) nitrate solution as a working fluid is investigated here. This cycle
415 permits the thermal potential of high temperature heat sources to be harnessed and used. The
416 operation of triple-effect cycles with the conventional working fluid H₂O/LiBr is not feasible at
417 temperatures of over 180°C due to the limited thermal stability and the high corrosiveness of the
418 working pair at high temperatures. The Alkitate topping cycle consists of a double-effect cycle in
419 parallel flow with H₂O/LiBr as a working fluid coupled with a high temperature single-effect cycle
420 using Alkitate as a working fluid. The results obtained from the Alkitate topping cycle are compared
421 with those obtained from the triple-effect cycle using H₂O/LiBr as a working fluid.

422 At the nominal operating conditions selected, namely a heat source temperature T_H of 250°C and a
423 cooling-water temperature T_C of 30°C the coefficient of performance achieved with the Alkitate
424 topping cycle is 1.73. The correct operation of the cycle is demonstrated by drawing the cycle in the
425 Duhring diagram, where the safety margin for the crystallization of the working fluid is adhered to.

426 The Triple-effect cycle with H₂O/LiBr as a working fluid shows COP values greater than those of the
427 Alkitate topping cycle up to T_H of 180°C, when COP trends are inverted as T_H increases leading to a
428 slightly higher performance of the Alkitate topping cycle. Moreover, it is worth mentioning that the
429 practical operation of H₂O/LiBr triple-effect cycles at temperatures of over 180 °C is not feasible due
430 to the limited thermal stability and the high corrosiveness of this working fluid at high temperatures.

431 Hence, the triple-effect cycle with a high temperature Alkitate stage represents a feasible and
432 efficient option to take advantage of the thermal potential of high temperature heat sources.

433 **Acknowledgements**

434 This study was part of an R&D project funded by the Spanish Ministry of Science and Innovation
435 (ENE2007-65541/ALT). M. Álvarez acknowledges the receipt of scholarship award (BES-2008-
436 006253) from the Spanish Ministry of Science and Innovation.

437

438 **References**

- 439 [1] Erickson D., Potnis S., Tang J., Triple effect absorption cycles, Proceedings of the 31st
440 Intersociety Energy Conversion Engineering Conference; 1996, Washington (USA), pp. 1072-1077.
- 441 [2] Mamiya, G. Multi-stage absorption refrigeration system. US Patent No. 3 831 397, 1974.
- 442 [3] Oouchi, T.; Usui, S.; Fukuda, T.; Nishiguchi, A. Multi-stage absorption refrigeration system. US
443 Patent No. 4 520 634, 1985.
- 444 [4] Ziegler F., Kahn R., Summerer F., Alefeld G, Multi-effect absorption chillers, International Journal
445 of Refrigeration 16 (1993), pp. 301-11.
- 446 [5] Grossman G, Wilk M, DeVault R., Simulation and performance analysis of triple-effect absorption
447 cycles. ASHRAE Transactions 100 (1994); pp.452-62.
- 448 [6] Garimella S., Lacy D., Stout R., Space-conditioning using triple-effect absorption heat pumps
449 Applied Thermal Engineering 17 (1997), pp. 1183-1197.
- 450 [7] Kaita Y., Simulation results of triple-effect absorption cycles, International Journal of Refrigeration
451 25 (2002), pp. 999-1007.
- 452 [8] Wang L., You S., Zhang H., Li X, Simulation of gas-fired triple-effect LiBr/water absorption cooling
453 system with exhaust heat recovery generator, Transactions of Tianjin University 16 (2010), pp. 187-
454 193.
- 455 [9] Gebreslassie B., Medrano M., Boer D., Exergy analysis of multi-effect water-LiBr absorption
456 systems: From half to triple effect, Renewable Energy 35 (2010), pp. 1773-1782.

- 457 [10] Gomri R., Investigation of the potential of application of single effect and multiple effect
458 absorption cooling systems, *Energy Conversion and Management* 51 (2010), pp. 1629-1636.
- 459 [11] Matsushima H., Fujii T., Komatsub T., Nishiguchi A., Dynamic simulation program with object-
460 oriented formulation for absorption chillers (modelling, verification, and application to triple-effect
461 absorption chiller), *International Journal of Refrigeration* 33 (2010), pp. 259-268.
- 462 [12] Agrawal B., Karimi, M., Thermodynamic performance assessment of a novel waste heat based
463 triple effect refrigeration cycle, *International Journal of refrigeration* 35 (2012), pp.1647-1656.
- 464 [13] Yabase H., Makita K., Steam driven triple effect absorption solar cooling system. *International*
465 *Refrigeration and Air Conditioning Conference at Purdue, USA, 2363* (2012) pp. 1-8.
- 466 [14] Geng C., Liu Y., Exergy analysis of a compressor assisted triple-effect absorption refrigerating
467 cycle, *Applied Mechanics and Materials* 405-408 (2013), pp. 2975-2979.
- 468 [15] Agrawal S., Kumar R., Khaliq A., First and second law investigations of a new solar-assisted
469 thermodynamic cycle for triple effect refrigeration, *International Journal of Energy Research* 38
470 (2014), pp. 162-173.
- 471 [16] Howe L., Erickson D., Proof-of-Concept Testing of Alktrate, Phase III. Final Report- Energy
472 Concepts Co., Annapolis, Maryland, USA, 1990.
- 473 [17] Alefeld, G.; Radermacher, R., *Heat conversion systems, USA, CRC Press Inc, 1994.*
- 474 [18] Grossman G., Zaltash A., ABSIM-modular simulation of advanced absorption, *International*
475 *Journal of Refrigeration* 24 (2001), pp. 531-543.

476 [19] Álvarez M.E., Theoretical and experimental study of the aqueous solution of lithium, sodium and
477 potassium nitrates as a working fluid in absorption chillers driven by high temperature heat sources
478 (in Spanish), PhD Thesis, Rovira i Virgili University, Tarragona, Spain, 2013.

479 [20] Gommed K., Grossman G., Performance analysis of staged absorption heat pumps: Water–
480 Lithium Bromide systems, ASHRAE Trans 1990, 96: 1590-1598.

481 [21] Boryta D., Solubility of lithium bromide in water between -50°C and 100 °C (45 to 70% lithium
482 bromide). Journal of Chemical Engineering & Data 15 (1970), pp. 142-144.

483 [22] Vargas P., Salavera D., Galleguillos H., Coronas A., Solubility of aqueous mixtures of alkaline
484 nitrates and nitrites determined by differential scanning calorimetry, Journal of Chemical Engineering
485 & Data 53 (2008), pp. 403-406.

486

487

488

489 Table 1. Input data for the simulation in ABSIM of the Alktrate topping cycle [5]

490 Input data	
491 Heat transfer characteristics (UA), kW.°C⁻¹	
491	Absorbers: ABS(2) and ABS(12) 6.11
	Generators: GEN(3), GEN(4) and GEN (13) 17.88
492	Condensers: CND(5), CND(6) and CND(14) 8.48
	Evaporators: EVP(1) and EVP(11) 11.90
493	Heat exchangers: HEX(7), HEX(8) and HEX(15) 2.03
494 Mass flow rates, kg.s⁻¹	
494	Absorbers (cooling-water): m ₃ and m ₅₂ 3.65
	Condensers (cooling water): m ₁₁ , m ₂₃ and m ₄₆ 2.96
495	Evaporator (chilled water): m ₂₈ and m ₅₄ 2.27
	Solution leaving the absorber ABS(2): m ₅ 0.45
496	Solution entering each generator: m ₈ , m ₁₃ and m ₃₃ 0.225
497 Temperatures, °C	
497	Heat source in GEN(13): T ₃₅ 250.00
	Inlet cooling-water: T ₃ and T ₂₃ 30.00
498	Outlet chilled water: T ₂₉ 7.20

499

500

501

502

503

504

505

506

507

508

509 **Table caption**

510

511 Table 1. Input data for the simulation in ABSIM of the Alktrate topping cycle [5]

512

513

514

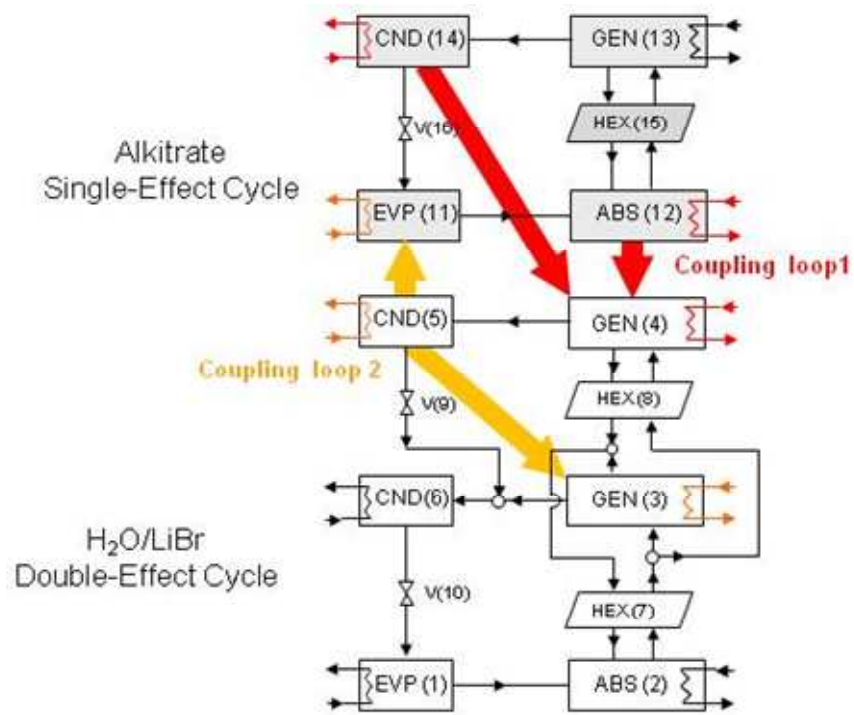
515

516

517

518

519



520

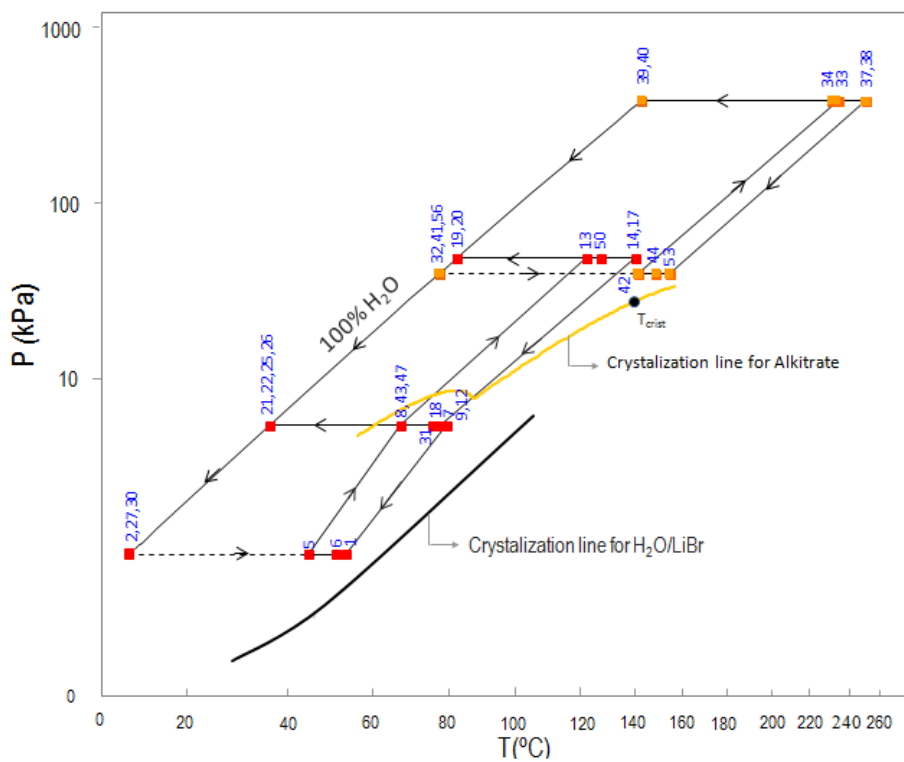
521 Figure 1. Configuration of the triple-effect absorption cooling cycle with a high temperature Alktrate
 522 stage

523

524

525

526

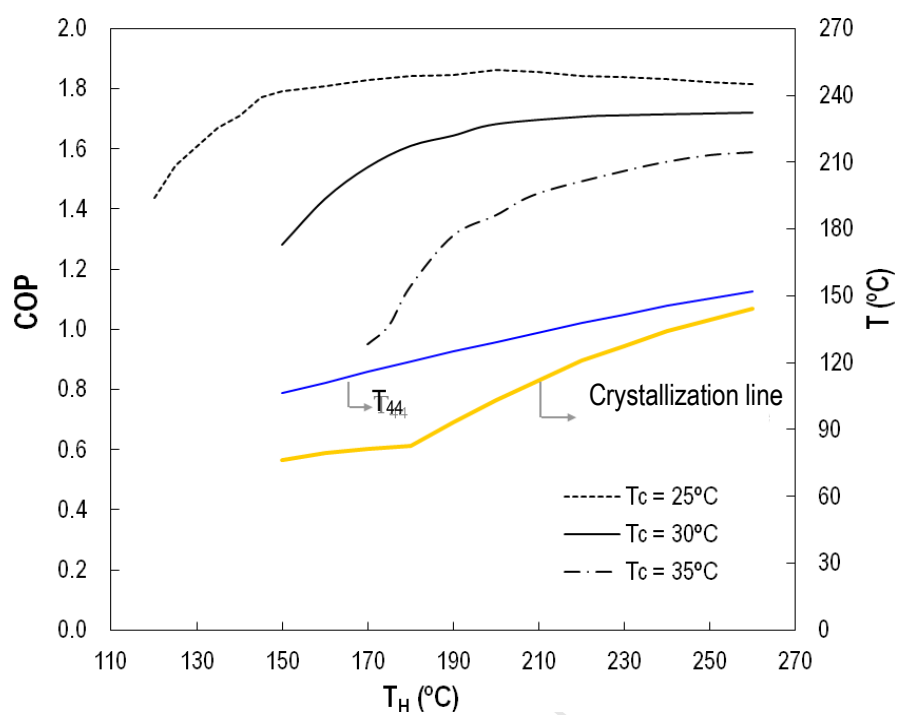


537

538 Figure 3. Dühring diagram (P-T-X) of the triple-effect absorption cooling cycle with a high
 539 temperature Alktrate stage at the operating conditions listed in Table 1

540

541

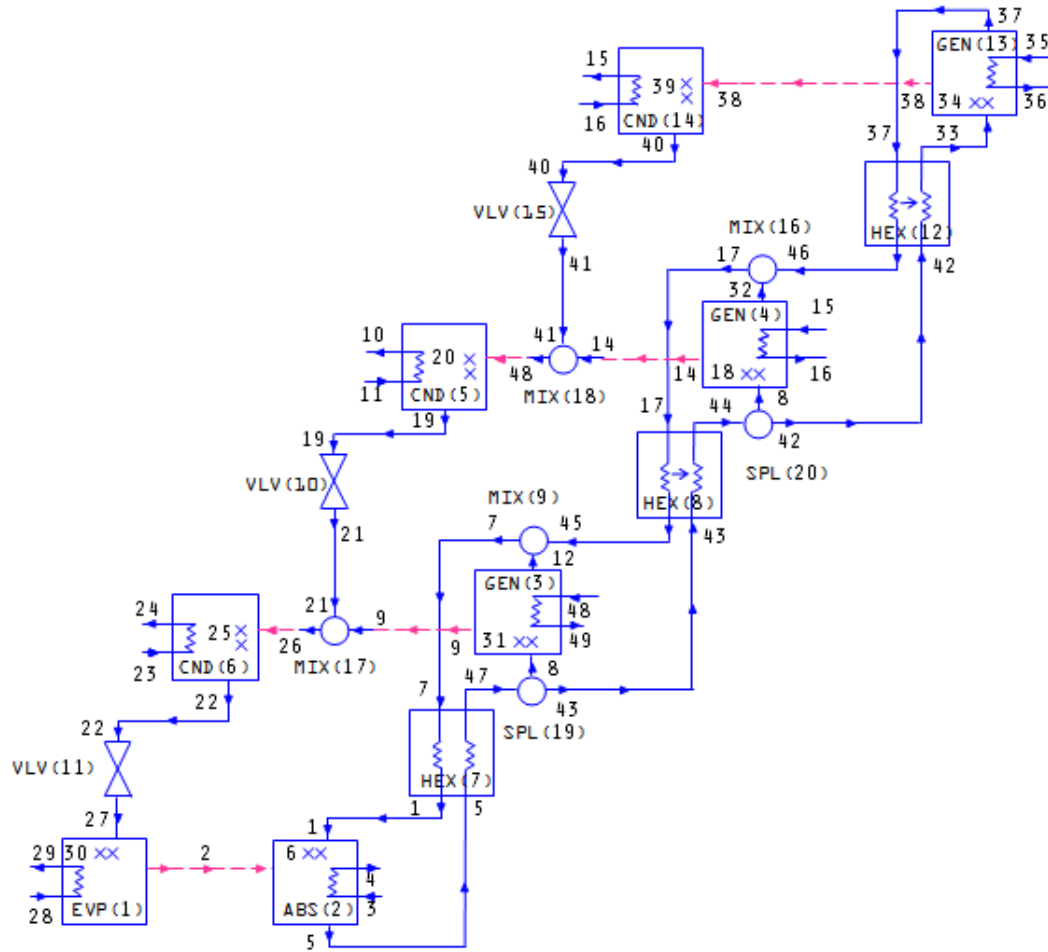


542

543 Figure 4. Coefficient of performance and crystallization line of the triple-effect absorption cooling
 544 cycle with a high temperature Alktrate stage, versus the temperatures of the heat source (T_H) and
 545 cooling-water (T_C)

546

547

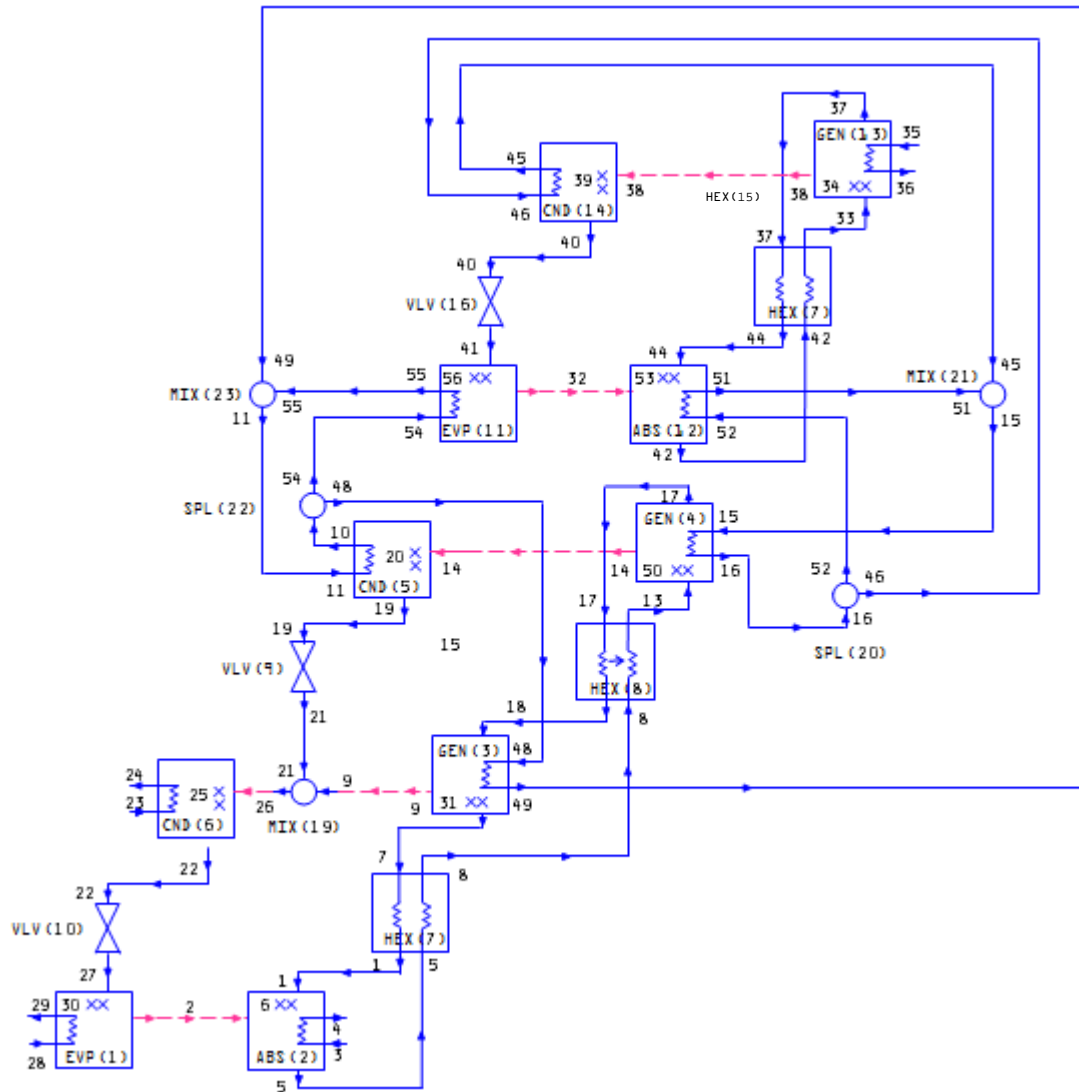


548

549 Figure 5. Configuration in ABSIM of the triple-effect absorption cooling cycle with two condensers

550 coupled alternatively in parallel flow [5]

551



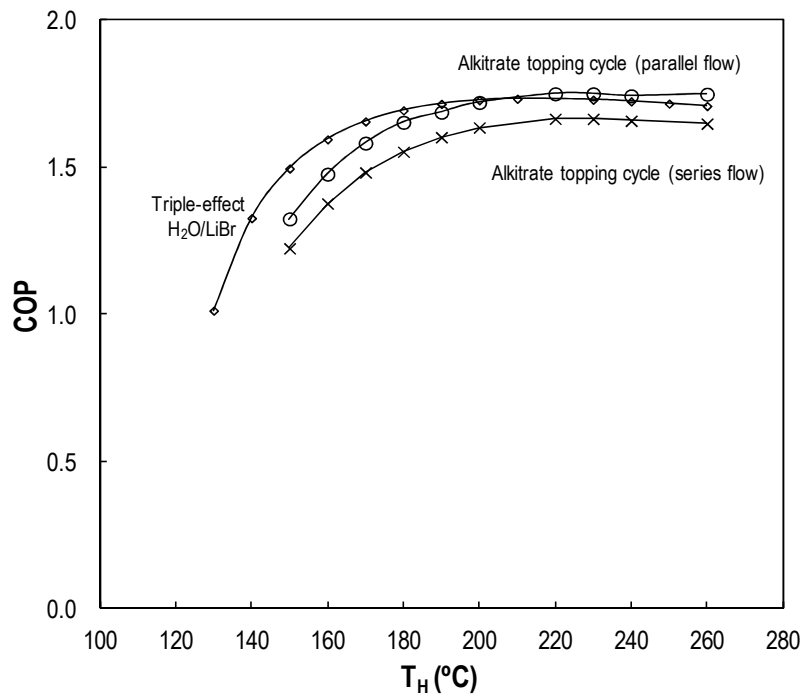
552

553 Figure 6. Configuration in ABSIM of the triple-effect absorption cooling cycle formed by a $\text{H}_2\text{O}/\text{LiBr}$
 554 series flow double-effect cycle and a single-effect using Alkitrane as a working pair

555

556

557

558
559

560 Figure 7. Coefficient of performance of the simulated absorption cooling cycles, H₂O/LiBr triple-effect
 561 cycles and parallel flow and series flow Alkitrane topping cycles, versus the heat source temperature
 562 T_H

563

564

565

566

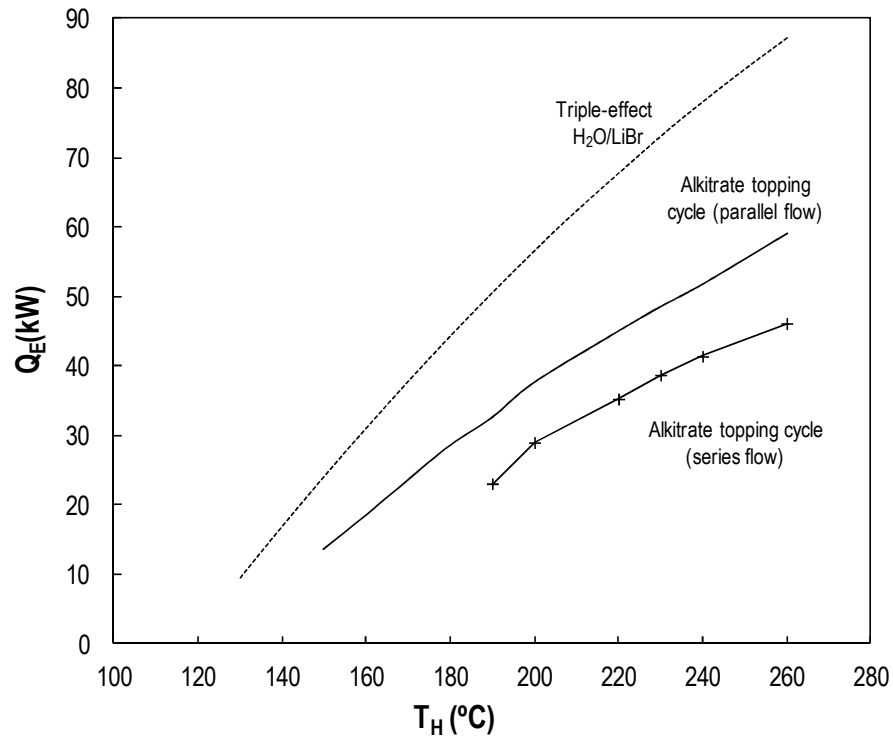
567

568

569

570

571



572

573 Figure 8. Cooling capacity of the simulated absorption cooling cycles, $H_2O/LiBr$ triple-effect cycles574 and parallel flow and series flow Alktrate topping cycles, versus the heat source temperature T_H

575

576

577

578

579

580 **Figures caption**

581 Figure 1. Configuration used in the present work for the triple-effect absorption cooling cycle with a
582 high temperature Alktrate stage

583 Figure 2. Configuration in ABSIM of the triple-effect absorption cooling cycle formed by a H₂O/LiBr
584 parallel flow double-effect cycle and a single-effect cycle using Alktrate as a working fluid

585 Figure 3. Dühring diagram (P-T-X) of the triple-effect absorption cooling cycle with a high
586 temperature Alktrate stage at the operating conditions listed in Table 1

587 Figure 4. Coefficient of performance and crystallization line of the triple-effect absorption cooling
588 cycle with a high temperature Alktrate stage, versus the temperatures of the heat source (T_H) and
589 cooling-water (T_C)

590 Figure 5 Configuration in ABSIM of the triple-effect absorption cooling cycle with two condensers
591 coupled alternatively in parallel flow [5]

592 Figure 6. Configuration in ABSIM of the triple-effect absorption cooling cycle formed by a H₂O/LiBr
593 series flow double-effect cycle and a single-effect cycle using Alktrate as a working pair

594 Figure 7. Coefficient of performance of the simulated absorption cooling cycles, H₂O/LiBr triple-effect
595 cycles and parallel flow and series flow Alktrate topping cycles, versus the heat source temperature
596 T_H

597 Figure 8. Cooling capacity of the simulated absorption cooling cycles, H₂O/LiBr triple-effect cycles
598 and parallel flow and series flow Alktrate topping cycles, versus the heat source temperature T_H

599